Available online at www.sciencedirect.com
ScienceDirect
Polymer 49 (2008) 241–253
polymer
www.elsevier.com/locate/polymer

Mixtures of tertiary amine functionalized azo-containing mesogens with acid-functionalized polymers

Carmen M. Tibirna*, Papa Niokhor Diouf

Centre de recherche en sciences et ingénierie des macromolécules (CERSIM), Département de chimie, and Centre de recherche sur le Bois (CRB), Département des Sciences du bois et de la forêt, Université Laval, Québec (QC), Canada G1K 7P4

Received 2 August 2007; received in revised form 1 November 2007; accepted 10 November 2007
Available online 19 November 2007

Abstract

A tertiary amine functionalized 4-nitro-4′-alkoxy azobenzene mesogen with a 10 or 12 carbon spacer (azo-*n*N) was synthesized and complexed in equimolar proportions with poly(acrylic acid) (PA−H) and poly(sulfonic acid) (PSS−H), and investigated by thermogravimetric analysis, differential scanning calorimetry, polarizing optical microscopy, Fourier transform infrared spectroscopy and X-ray diffraction. The neat azo-*n*N is characterized by a partial bilayer S_A mesophase at higher temperatures, and a highly ordered phase, in which the molecules are stacked orthogonally in bilayers, at lower temperatures. As supported by infrared analysis, for the azo-*n*N/PA−H mixture, the complexation is partial while for the same azo-*n*N/PSS−H mixture, complete proton transfer occurs. When the azo-*n*N is blended with the PA−H, regarded as a weak acid, a biphasic system is generated and the thermotropic behavior of neat mesogen is not significantly affected. In contrast, by mixing the same mesogen with a PSS−H (regarded as a strong acid), the thermotropic behavior is significantly influenced: the complexation generated a partial or interdigitated smectic A or tilted smectic C lamellar phase.

Keywords: Liquid crystalline polymers (LCP); Azo mesogens; Surfactants−polymers complexes

1. Introduction

Supramolecular side chain liquid crystal polymers (SCLCPs), which combine the mechanical properties of a polymer and conventional properties of low molecular weight liquid crystals, are an elegant and very useful class of materials for non-linear optics [1], optical data storage [2] and display materials [3]. Among the different molecular engineering approaches used in the design of such materials, the specific non-covalent interactions are the most attractive. Various groups [4–8] have studied supramolecular side-chain type polymers formed by hydrogen-bonding interactions between a low molar mass molecule functionalized at one end and a complementary functionalized polymer. Such systems include surfactant−polyelectrolyte complexes where the thermotropic mesogenic moieties are incorporated in the surfactant and the polyelectrolytes are available polymers. In this regard, terminal amine groups, and particularly tertiary amines, can interact with acidic polymers such as poly(acrylic acid) (PA−H), poly(methacrylic acid) (PMA−H), poly(styrenesulfonic acid) (PSS−H), etc. Bazuin and Tork [9,10] have reported side-chain supramolecular LCPs obtained by proton-transfer interactions (2:1 acid/amine complexation) between diethylamine-functionalized alkoxy biphenyl mesogens (LC-1,*n*N) and PA−H.

We have previously reported [11] the results of our investigation of an ionic system, involving a triethyl-ammonium functionalized-4-nitro-4′-alkoxy azobenzene mesogen and different oppositely charged polyelectrolytes. We found that the functionalized low molar mass mesogen is highly ordered. By mixing this mesogen with amorphous, commercially available polyelectrolytes a disordered liquid crystalline mesophase over a very wide temperature range was generated, through ionic complexation. Continuing and extending the study in

* Corresponding author. Tel.: +1 418 658 2286; fax: +1 418 656 2091.
E-mail address: carmen.tibirna@sbf.ulaval.ca (C.M. Tibirna).

0032-3861/$ - see front matter © 2007 Elsevier Ltd. All rights reserved.
doi:10.1016/j.polymer.2007.11.026

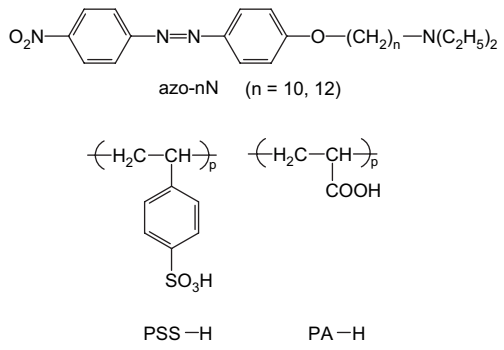

Fig. 1. Molecular structures of the mesogens and functionalized polymers used in this study.

this field, we present in this paper a thermal and structural investigation of a comparable functional polymer–mesogen system but involving other strong non-covalent interactions, the H-bonds. Particular characteristics of our adopted molecular architecture are that the intermolecular hydrogen bonds are located near the polymer backbone, the flexible spacer is part of the functionalised mesogen and the chromophore is a conjugated π-electron donor–acceptor system. The mesogens used possess a rigid azobenzene core, are tertiary amine-capped and act as H-bond acceptors. They will be referred to as azo-*n*N (*n* is the number of carbons in the spacer and N refers to the amine functionality). Two simple acidic polymers, PA–H and PSS–H, were used in this study that are, respectively, functionalized with carboxylic and sulfonic acid, and operate as H-bond donors. The chemical structures of the two constituents are shown in Fig. 1. The aim of this work is to synthesize and characterize the mesogens and to investigate the relationship between the chemical structure of polyacid–amine mixtures in the bulky state and their ability to form ordered mesomorphic phases. The effect of spacer length on the properties of the system has also been examined.

2. Experimental section

2.1. Materials

All of the reagents and polymers were obtained from Aldrich Chemical Co. 4-Nitroaniline (99%), phenol, sodium nitrite, 1,10-dibromodecane, 1,12-dibromododecane, chloroform, acetone, ethanol, ethylacetate, diethylamine, sodium sulfate, hexanes, all of the best reagent grades available, were used as received. Poly(acrylic acid) (PA–H) in powder form, obtained from Aldrich and reported to have a molar mass of 250,000, was also used as received. Sodium poly(styrene sulfonate) (PSS–Na), reported to have a molecular weight of 70,000, was acidified in order to prepare PSS–H by ion exchange according to the method described in the literature [12]. PSS–Na was deionised by passage through a column in which an ion-exchange resin (DOWEX 50WX4-50) was packed. The aqueous solution of this polymer was freeze-dried and then the resulting product was dried in vacuo at about 65 °C for a week. The elimination of the Na ions was qualitatively verified by an energy dispersive X-ray spectrometer (EDS) coupled to a scanning electron microscopy (SEM), and by infrared spectroscopy. Column chromatography was performed using silica gel (Aldrich, 70–230 mesh), and thin-layer chromatography was carried out on silica gel plates (Aldrich, 200 μm).

2.2. Synthesis of chromophore azo-nN

The sequence of reaction for the synthesis of the azo-*n*N chromophores ($n = 10,\ 12$) involves three main steps, as shown in Fig. 2.

2.2.1. 4-Nitro-4′-hydroxyazobenzene (*I*)

In accordance with literature procedures [13], 4-nitroaniline (20 g, 0.145 mol), was added to a warm solution of concentrated hydrochloric acid (50 ml) and water (50 ml). The solution was cooled and maintained at about 5 °C using an ice/salt bath. For the diazotation, a mixture of sodium nitrite (10 g, 0.145 mol) and water (30 ml) was added to the cold solution. The end of reaction was verified by potassium iodide–starch paper. The diazonium salt was slowly added under stirring to an ice-cooled mixture of phenol (13.6 g, 0.145 mol) and sodium hydroxide (28 g) in water (100 ml). The reaction mixture was stirred for 1 h at about 5 °C, and was then acidified with concentrated hydrochloric acid. The precipitate was filtered, washed ten times with water and dried. The product (**I**) formed was recrystallized twice from ethanol/water (80:20 v/v). Yield: 21.5 g (61%) in the form of dark red crystals. ^{1}H NMR ($CDCl_3$, TMS, 25 °C): $\delta = 7.00$ (d, 2H, Ar–O–), 7.9 (m, 4H, Ar–N=), 8.4 (d, 2H, Ar–NO_2).

2.2.2. n-Bromo-1-((4-((4-nitrophenyl) azo)phenyl)oxy)alkane (*II*) [14]

Product **I** (10 g, 0.041 mol) and an excess of potassium carbonate were stirred in acetone (125 ml). To this, 1,*n*-dibromoalkane (0.041 mol) was added and the reaction mixture was heated under reflux for 100 h. The precipitated potassium bromide was filtered out, and the acetone was removed by

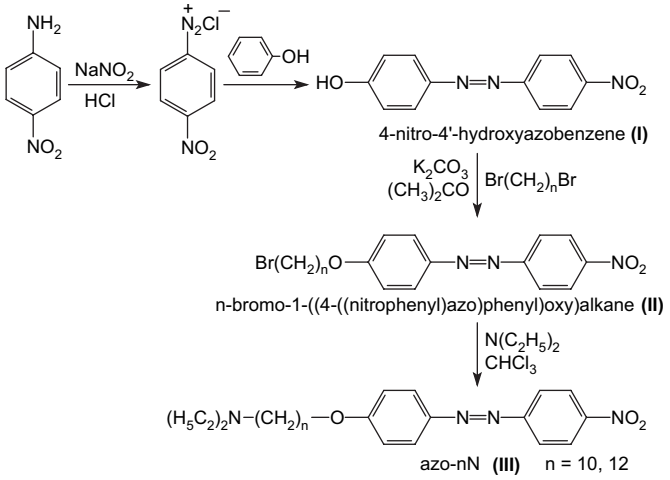

Fig. 2. Synthetic route for the azo-*n*N mesogens' preparation.

rotary evaporation. The crude product was dissolved in chloroform, and the chloroform solution was extracted ten times with water and evaporated. Purification was performed by recrystallization from ethanol. Yield: 46% in the form of a red crystalline solid. ^{1}H NMR ($CDCl_3$, TMS, 25 °C): $\delta = 1.25-1.65$ (m, 8H, inner $-CH_2-$), 1.8 (m, 4H, $Br-CH_2-CH_2-$ and $-O-CH_2-CH_2-$), 3.4 (t, 2H, $Br-CH_2-CH_2-$), 4.0 (t, 2H, $O-CH_2-CH_2-$), 7.0 (d, 2H, Ar–O–), 8.00 (m, 4H, Ar–N=), 8.4 (d, 2H, $Ar-NO_2$).

2.2.3. 4-(γ-bis-2-ethyl)aminoalkoxy-4′-nitroazobenzene or azo-nN (III)

Product **II** (0.01 mol) and diethylamine (0.1 mol) were dissolved in chloroform (100 mL). The reaction mixture was heated under reflux for one week, and then the solvent was evaporated. The crude product was re-dissolved in chloroform, and excess diethylamine and HBr were removed by water extraction. The chloroform phase was dried by anhydrous sodium sulfate. The solvent was evaporated and the resulting product was recrystallized at least twice from a mixture of ethyl acetate and hexane (80:20 v/v). Any unreacted precursor was removed in this step. The purity of the products (azo-*n*N) was verified initially by thin-layer chromatography using ethyl acetate as a mobile phase. The pure mesogens were dried in vacuo at about 65 °C for a week. The yield of the procedure was 49%. Both mesogens are brown-red in color and are soluble in chloroform and ethyl acetate at ambient temperature as well as in hot ethanol and methanol. They are not soluble in benzene, toluene or hexane. The purity of the azo-*n*N was confirmed by elemental analysis (Table 1) and ^{1}H NMR spectroscopy after drying the samples in vacuo for 6 days at 65 °C. ^{1}H NMR spectra ($CDCl_3$, TMS, 25 °C): azo-*n*N ($n = 10$ and 12), $\delta = 8.35$ (d, 2H, $Ar-NO_2$), 7.91 (m, 4H, Ar–N=), 7.00 (d, 2H, Ar–O–), 4.00 (t, 2H, $O-CH_2-CH_2-$), 2.52 (q, 4H, $N-CH_2-CH_3$), 2.43 (t, 2H, $N-CH_2-CH_2-$), 1.80 (m, 2H, $O-CH_2-CH_2$), 1.2–1.6 [m, $(2n-6)$H, CH_2 aliphatic], 1.04 (t, 6H, $N-CH_2-CH_3$).

2.3. Preparation of the azo-nN/polymers mixtures

Three stoichiometric mixtures (azo-10N with PA–H and PSS–H; azo-12N with PSS–H) were prepared, using the following procedure. The two accurately weighed components were first dissolved separately in a common solvent [hot ethanol (EtOH)], which gave clear solutions. After stirring for 30 min, the azo-*n*N mesogen solution was added all at once to the polymer solution, to give a final solution of about 1% concentration. A very fine precipitate formed immediately, giving a cloudy solution, with no further change over time: this behavior is a sign of complexation [9]. After one day of reflux, the solvent was removed by evaporation. The resulting product was further dried in a vacuum oven at about 65 °C for one week.

Table 1
Elemental analysis of the azo-*n*N mesogens

n	Empirical formula	%C		%H		%N	
		Calcd.	Found	Calcd.	Found	Calcd.	Found
10	$C_{26}H_{38}O_3N_4$	68.69	68.15	8.42	8.56	12.32	11.40
12	$C_{28}H_{42}O_3N_4$	69.68	69.67	8.77	8.93	11.60	11.50

2.4. Techniques of analysis

The ^{1}H NMR spectra were recorded at 25 °C on a 300 MHz Bruker AC-300 spectometer using $CDCl_3$ as solvent. Elemental analysis was performed at the University of Montreal (Chemistry Dept.).

Scanning electron microscopy observations were carried out with a JEOL-840A instrument coupled with a Tracor-Northern TN 8502/S image analyzer. In addition to conventional secondary and back scattered electron detectors, this microscope is equipped with an energy dispersive X-ray spectrometer (EDS). The associated NORAN–EDS system was used for determination of elemental chemical composition of the samples. To obtain conductive samples, required for this analysis, the samples were glued to an aluminium stub and coated with a very thin layer of Pd/Au alloy.

Thermogravimetric analysis (TGA) was carried out under constant nitrogen flow (200 ml min^{-1}) at a heating rate of 10 °C/min using a Mettler TGA-50 balance. The samples were previously dried for 3 days in vacuo at 80 °C, and in situ at 50 °C for 10 min just prior to heating scans. The temperature of thermal degradation was determined at the onset of deviation from the plateau (T_d^{onset}) and at the point of 5% weight loss relative to the weight at 100 °C ($T_d^{5\%}$).

Thermal characterization was performed using a Perkin–Elmer DSC-7 differential scanning calorimeter (DSC), calibrated with indium and flushed with nitrogen. The heating and cooling scans were performed at 10 °C/min, on 5–15 mg of sample dried in vacuo for 3 days at 65 °C prior to packing into standard aluminium pans. First-order transition temperatures are given by the peak values, and glass transition temperatures (T_g) by the midpoint of the heat capacity jump of the second or third heating scan.

Polarized optical microscopy (POM) observations of samples sheared into thin films between two glass slides were made with a Zeiss Axioskop polarizing optical microscope equipped with a 25× Leica objective and a Hitachi 3 CCD HV-D27 camera. The temperature was regulated using a Mettler FP5 or FP80 temperature controller and a Mettler FP52 or FP82 hot stage.

X-ray diffractograms were obtained using a Bruker diffractometer equipped with a Kristalloflex 760 sealed-tube copper anode generator, operated at 40 kV and 40 mA, and a two-dimensional position-sensitive wire–grid detector (Bruker AXS) pressured with xenon gas. Collimation was effected by a graphite monochromator with a 0.8-mm pinhole. Data in the range of $2\theta = 0.9-27°$ were obtained using a home-made off-centered 5-mm beam stop and a sample-to-detector distance of 9 cm. Temperature was regulated by an Instec HCS 400 oven coupled with a STC 200D controller. Samples, previously dried in vacuo at 80 °C for 3 days, were placed in sealed Mark-Röhrchen glass capillaries (Charles Supper) of

0.5 or 1.0 mm inner diameter. All images were treated by subtracting a baseline image obtained using an empty capillary tube. The two-dimensional image was then integrated (generally over 360° for azo-*n*N and over 180° for the mixtures) to plot the intensity as a function of 2θ. The *d*-spacings were determined from the maximum of the diffraction peaks in the smoothed diffractograms, using the Bragg formula, $d = n\lambda/(2\sin\theta)$, where n is an integer giving the order of the diffraction peak, θ is the angle of incidence and λ is the wavelength of the X-ray beam used (Cu Kα, $\lambda = 0.1542$ nm).

Extended molecular lengths (l_C) of the chromophores were calculated using Hyperchem 5 (Hypercube Inc.) for the lowest energy conformation of the molecules with the methylene units in an *all-trans* conformation (including Van der Waals' radii at the extremities). The contribution of the polymer and the hydrogen bonds will be described in the Section 3.

Fourier transform infrared (FTIR) spectra were obtained from an accumulation of 400 scans at 4 cm^{-1} resolution at room temperature, using a Magna Nicolet 650 FTIR spectrometer equipped with a mercury–cadmium–tellurium detector. Samples were analyzed in the form of KBr (FTIR grade, Aldrich) pellets. The treatment of the FTIR spectra was done using Grams 5.1 (Galactic Industries).

3. Results and discussion

3.1. Verification of acidification of polymers

The successful elimination of the Na ions was qualitatively observed by EDS. This is illustrated by the absence of Na signal in the EDS spectrum, after ion exchange process of PSS–Na yielding PSS–H, shown in Fig. 3b by comparison of PSS–Na spectrum (Fig. 3a).

FTIR spectra of PSS–Na and PSS–H are compared in Fig. 4 and they indicate that complete acidification was achieved in the sample. When the Na ions are exchanged for H in the PSS sample, a number of infrared spectral changes were observed, generally similar to that reported in hydrated poly[styrene-co-(styrenesulfonic acid)] (PS–SSA) [15–17] and in metal-neutralized PS–SSA [15]. A first evidence of acidification is the band located at about 886 cm^{-1} in the PSS–H spectrum and absent in the PSS–Na spectrum. This band is assigned to the stretching vibration of the SO bond with single-bond character in the SO_3H group. In the same spectrum another change is observed for the 1172 cm^{-1} symmetric vibration of the acid that seems to be transformed into a doublet around 1200 cm^{-1}, related to the antisymmetric vibration of the $-SO_3^-$ ion. In addition, for PSS–Na the symmetric $-SO_3^-$ vibration is found in the region 1040 cm^{-1} while in the spectrum of PSS–H, this symmetric stretching vibration of the two SO bonds with double bond character (O=S=O) is located at 1172 cm^{-1}. The band located at 1352 cm^{-1} is assigned to the antisymmetric stretching vibration of SO_2, whereas a band near 1120 cm^{-1} is attributed to in-plane skeleton vibrations of the benzene ring with strong participation of the substituents. Another band is found at 1005 cm^{-1} and is attributed to in-plane bending vibrations of the benzene ring substituted in the *para* position, and also reflects the degree of ionization of the acid groups present. The intensity of this band and the intensity ratio of the 1005 cm^{-1} to the 1040 cm^{-1} band are higher in the PSS–H spectrum than in that of PSS–Na.

3.2. Thermal and structural characterization of the azo-nN mesogens

The thermal stability of the azo-*n*N mesogens and azo-*n*N/P–H stoichiometric mixtures under nitrogen atmosphere was examined by thermogravimetric analysis (TGA). The results are shown in Fig. 5. It can be observed that thermal

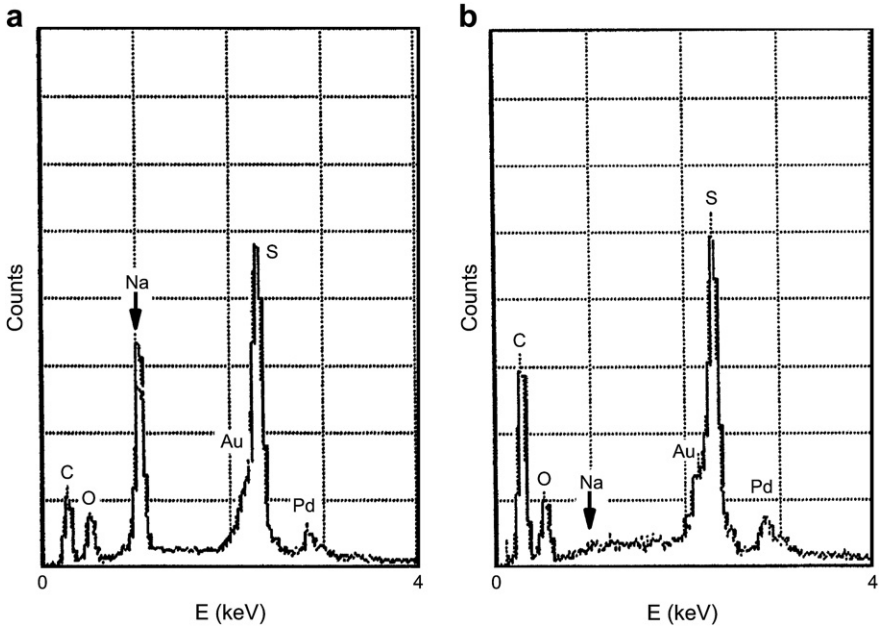

Fig. 3. EDS spectra of (a) PSS–Na (supplied by Aldrich) and (b) PSS–H (after ion exchange).

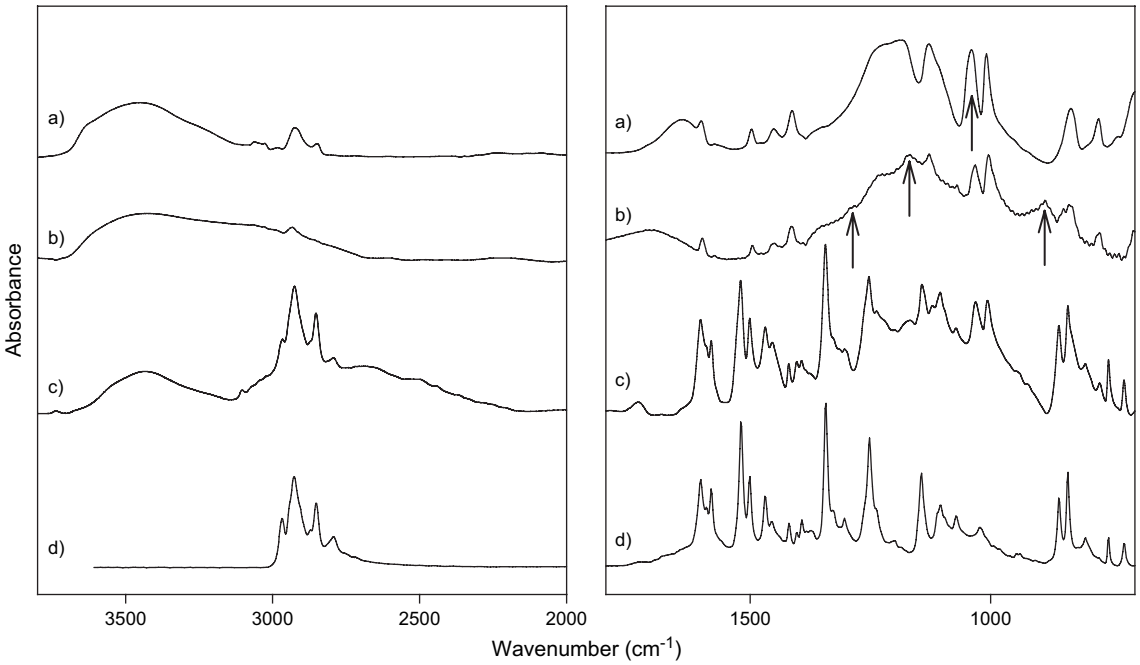

Fig. 4. FTIR spectra of (a) PSS–Na; (b) PSS–H; (c) equimolar azo-10N/PSS–H mixture and (d) pure azo-10N.

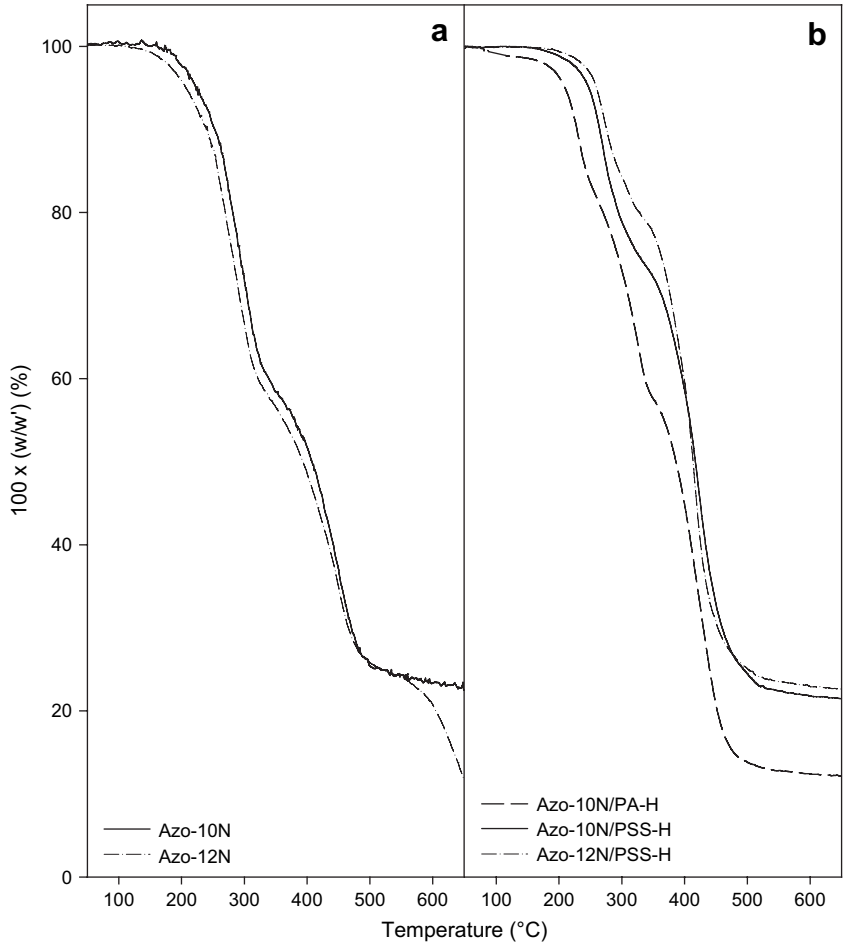

Fig. 5. Thermogravimetric scans under nitrogen of (a) pure azo-*n*N mesogens and (b) equimolar azo-*n*N/P–H (1:1) mixtures (weight, *w*, relative to weight, *w*′, at 100 °C).

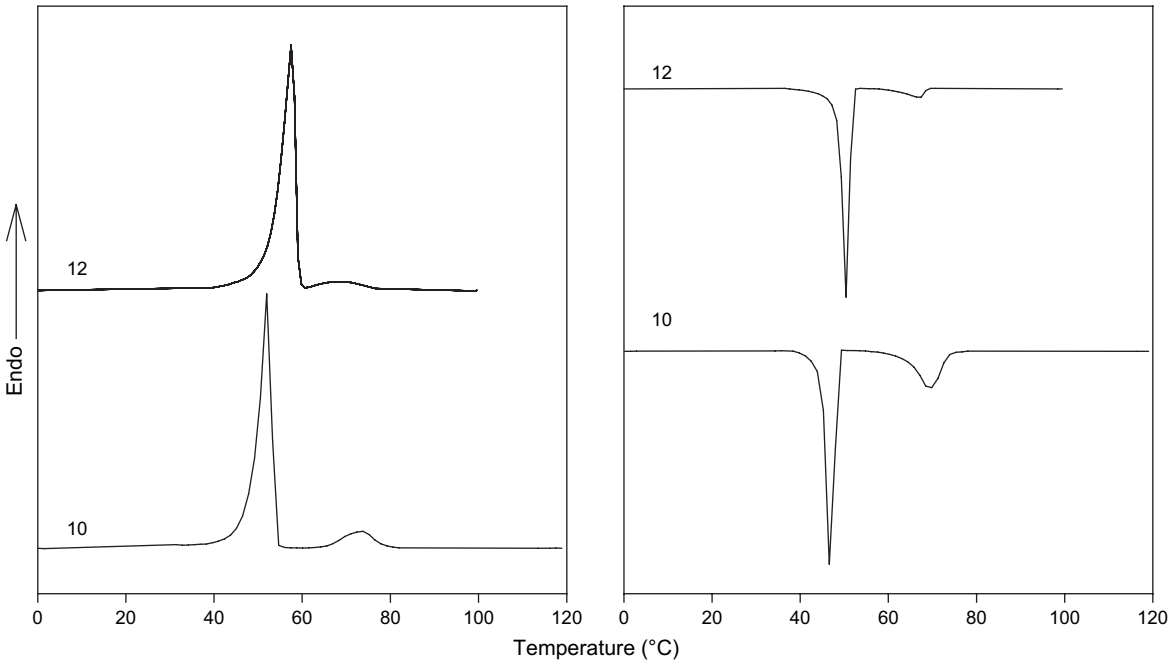

Fig. 6. DSC traces of the azo-*n*N at 10 °C/min (with *n* indicated for each plot).

degradation of the azo-*n*N mesogens occurs in two main steps. Azo-10N is slightly more stable (by about 15 °C) than azo-12N. Degradation appears to begin near 150 °C, with 5% weight loss occurring above 200 °C.

In DSC studies, the maximum temperature scanned was limited to be below the onset of sample degradation according to dynamic TGA analysis. Representative DSC traces for the azo-*n*N mesogens on both heating and cooling are shown in Fig. 6. The heating curves of azo-10N mesogen consist of two sharp endothermic peaks: an intense one at 52 °C ($\Delta H_1 = 61$ J/g) and a weaker one at about 20 °C higher ($\Delta H_2 = 10$ J/g). Both transitions are reversible on cooling, and exhibit only a small amount of supercooling. Thermograms of the azo-12N are similar. For these two mesogens, the strong transition is higher in temperature for the longer mesogen, whereas the opposite is true for the weak transition.

POM observations revealed that the first peak can be associated with a transition from a crystal to a liquid crystalline phase and the second peak can be identified as a transition from the liquid crystalline to the isotropic phase. When the azo-10N is cooled from the isotropic phase, the texture shown in Fig. 7a, resembling to small individual spherulites, first appears. On further cooling, at about 40 °C, it slowly develops into the texture shown in Fig. 7b. A spherulitic texture like that shown in Fig. 7a was observed by Tork [18] for a transition from an isotropic phase to an S_A phase in a diethylamine-functionalized cyano-biphenyl mesogen. The phase is clearly a liquid phase that spontaneously moves and yields easily under pressure.

Fig. 8 shows the X-ray profiles obtained for the azo-*n*N mesogens ($n = 10$, 12) at various temperatures. At ambient temperature, the wide angle region of the powdered samples is typical of a highly ordered crystalline phase, in accordance with the DSC data. At small angles, two (for azo-12N) or three (for azo-10N) diffraction peaks are observed and they can be assigned to the first- and second-order reflections, respectively, of a lamellar morphology. It can also be observed that the second-order peak is the most intense and it may be related

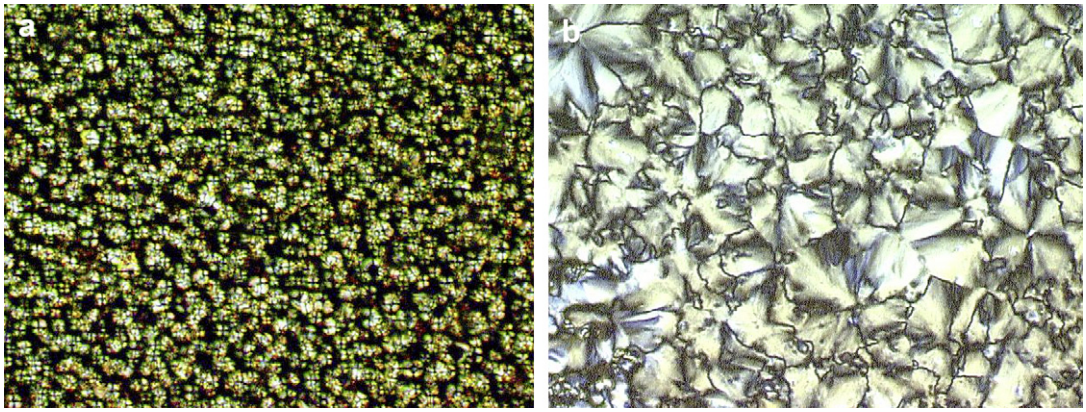

Fig. 7. Polarizing optical micrographs of azo-10N at (a) 50 °C and (b) 25 °C after slow cooling (3 °C/min) from the isotropic phase.

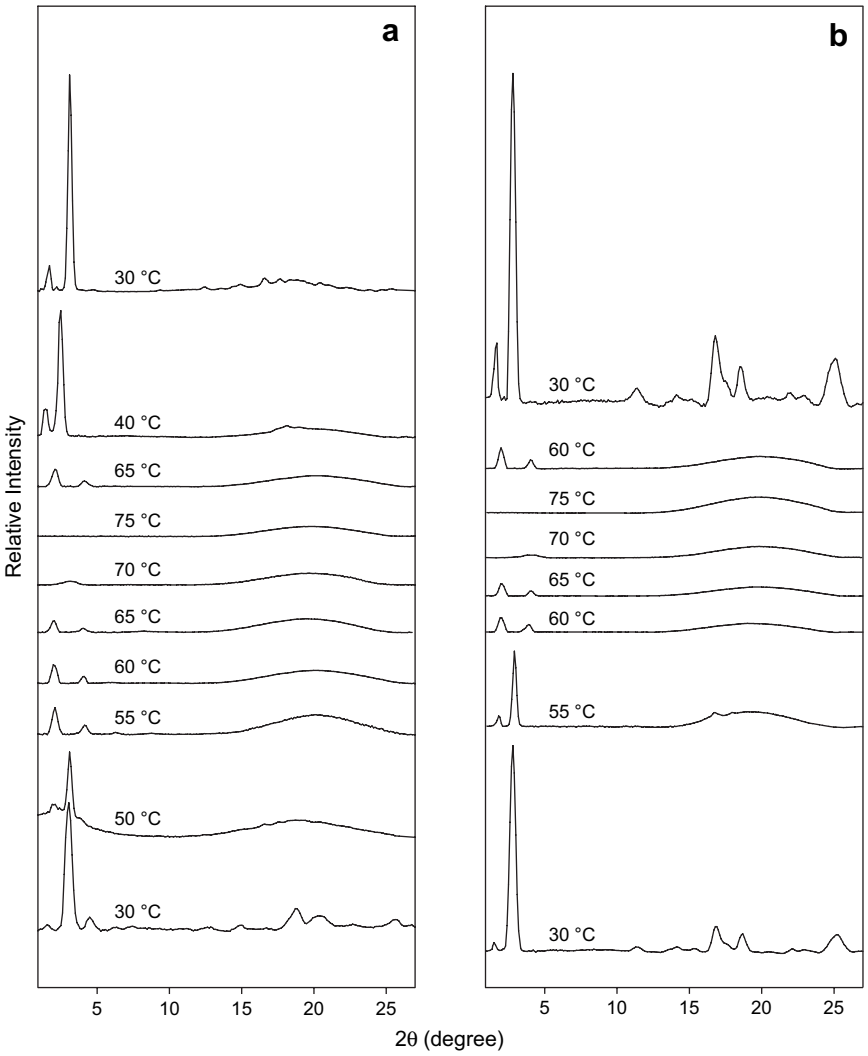

Fig. 8. X-ray diffraction profiles of (a) azo-10N and (b) azo-12N mesogens obtained upon heating and cooling (in order from bottom to top).

to an additional plane of symmetry in the lamellar electron density profile [19]. In the high-temperature mesophase, the X-ray diffractograms of the azo-*n*N mesogens are consistent with the smectic A or C assignment: a broad halo centered at about 20°, characteristic of disordered alkyl chains and corresponding to a Bragg spacing of about 4.5 Å, is accompanied by two or three sharp small angle diffraction peaks with reciprocal spacing in the ratio 1:2:(3). All of these peaks shift slightly to higher 2θ angles with increasing temperature. This effect is frequently observed for orthogonal lamellar materials and is associated with thermal motion which creates a greater disorder and induces a decrease of lamellar thickness.

The Bragg distances determined from the small angle diffraction data and extended molecular lengths are given in Table 2. At ambient temperature, the lamellar thicknesses are twice the length of the mesogens in their most extended conformation. This indicates that the mesogens are packed at ambient temperature in a bilayer lamellar crystalline phase. The lamellar thickness of the high-temperature phase is between one and two calculated molecular lengths in their most extended conformation. This suggests a partial bilayer phase with interdigitation of the molecules in an orthogonal phase (smectic A) or possibly tilting of the mesogenic long axis relative to the layer normal (tilted smectic C bilayer).

In summary, the azo-*n*N mesogens are thermotropic liquid crystals, characterized by a partial bilayer S_A mesophase at higher temperatures, and a highly ordered phase, in which the molecules are stacked orthogonally in bilayers, at lower temperatures.

3.3. Characterization of azo-nN/P–H mixtures

3.3.1. FTIR analysis

In order to qualitatively evaluate the state of complexation between the components in the azo-*n*N/P–H mixtures, FTIR analysis was performed. A FTIR spectrum of the stoichiometric azo-10N/PA–H mixture is compared in Fig. 9 with those of pure PA–H as well as pure azo-10N. Our results can be compared with those obtained by Tork and Bazuin [9] for LC-1,*n*N/PA–H system. In their system, the partial proton transfer from the acid to the amine moieties was indicated by the strong reduction of the acid carbonyl band (dimer form) near 1710 cm^{-1} compared

Table 2
Bragg spacings of the azo-*n*N chromophores, as determined experimentally from the small angle X-ray diffraction data (d_1, d_2, d_3), and compared with the calculated molecular lengths in extended conformation (l_c)

Temperature (°C)	Azo-10N ($l_C = 30.8$ Å)				Azo-12N ($l_C = 33.3$ Å)		
	d_1 (Å)	d_2 (Å)	d_3 (Å)	d_w (Å)	d_1 (Å)	d_2 (Å)	d_w (Å)
30[a]	58.9	29.4	19.6	–	63.1	31.5	–
50[a]	46.5	28.5	–	–	[c]	[c]	[c]
55[a]	44.8	21.9	–	4.5	48.8	24.9	–
60[a]	43.3	21.5	–	4.5	46.5	28.5	4.5
65[a]	42.3	21.4	–	4.5	44.2	22.1	4.5
70[a]	28.3	–	–	4.5	–	–	4.5
75[a]	–	–	–	4.5	–	–	4.5
65[b]	42.5	21.5	–	4.5	[c]	[c]	[c]
60[b]	[c]	[c]	[c]	[c]	44.8	22.1	4.5
40[b]	60.9	31.5	–	–	[c]	[c]	[c]
30[b]	55.5	28.5	–	–	62.2	31.5	–

[a] Heating.
[b] Cooling.
[c] Not measured.

to what is observed in the LC-1,12Br/PA–H spectrum (where there is no proton transfer). Another evidence of partial complexation was the appearance in the mixtures of new absorption band at about 1550 cm^{-1} assigned to the asymmetric COO^- stretch. As illustrated in Fig. 9, the residual carbonyl absorption in our equimolar complex indicates that some uncomplexed mesogen remains.

Further comparison of the spectra presented in Fig. 9 reveals that a new weak band near 2650 cm^{-1} and a very weak band near 2500 cm^{-1} appear in the azo-10N/PA–H mixture, and may be attributed to the (hydrogen-bonded) protonated amine moiety ($^+HEt_2N–$, $–CO_2^-\cdots{}^+HEt_2N–$) [20]. Other differences between the spectrum of the azo-10N and that of the azo-10N/PA–H mixture are noted for the ethyl band at 2798 cm^{-1} and the C–N band at about 1200 cm^{-1}, which decrease in intensity in the azo-10N/PA–H mixture compared to the pure azo-10N. Since several studies indicate that tertiary amine functionalized small molecules complexate about 50% of the acid groups in PA–H [6,9,10] it can be assumed that this is the case also for the present mixtures with PA–H.

Fig. 4 compares the FTIR spectra of the equimolar azo-10N/PSS–H mixture with pure azo-10N, PSS–H and PSS–Na. It indicates that complete proton transfer from the polymer acid to the amine groups of the functionalized mesogen occurs in this case. The most obvious change is the disappearance of the acid-related band located at about 886 cm^{-1}. Similar behavior is observed in sodium salt of the polymer alone in this spectral region and confirms the complete protonation of sulfonate groups in the azo-10N/PSS–H mixture. Another difference indicative of proton transfer in the spectrum of azo-10N/PSS–H is noted in the 2500–3600 cm^{-1} region. A new weak band near 2650 cm^{-1} and a very weak band near 2500 cm^{-1} appear in the mixture and may be attributed to the (hydrogen-bonded) protonated amine moiety ($^+HEt_2N–$, $SO_3^-\cdots{}^+HEt_2N–$).

3.3.2. Thermal characterization

Thermogravimetric analyses of the azo-10N/P–H and azo-12N/PSS–H mixtures are shown in Fig. 5b. The carboxylated mixture (azo-10N/PA–H) shows an initial weight loss of about 2% between 100 and 150 °C, which may be due to the removal of residual H_2O. Taking the onset of degradation to occur at the end of the plateau beyond this initial loss, or referring to the 5% degradation values, it can be observed that this mixture is the least stable of the three, and similar to that of the pure

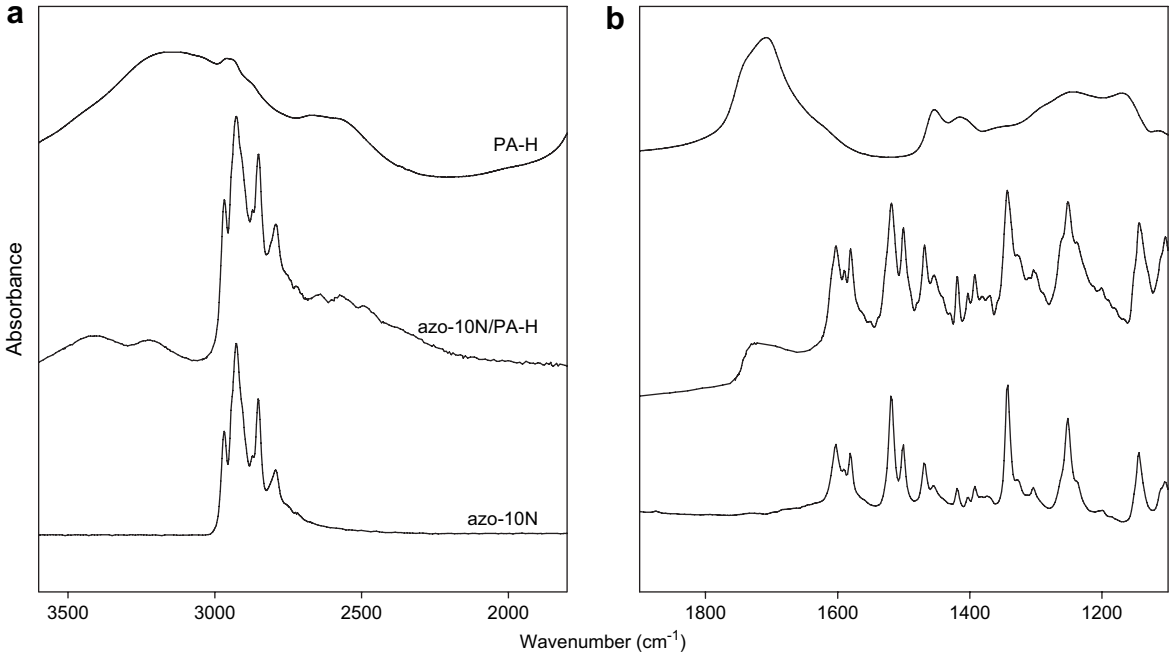

Fig. 9. Ambient temperature infrared spectra (a) from 1800 to 3600 cm^{-1} and (b) from 1100 to 1900 cm^{-1} of pure azo-10N, the equimolar mixture of azo-10N/PA–H, and pure PA–H.

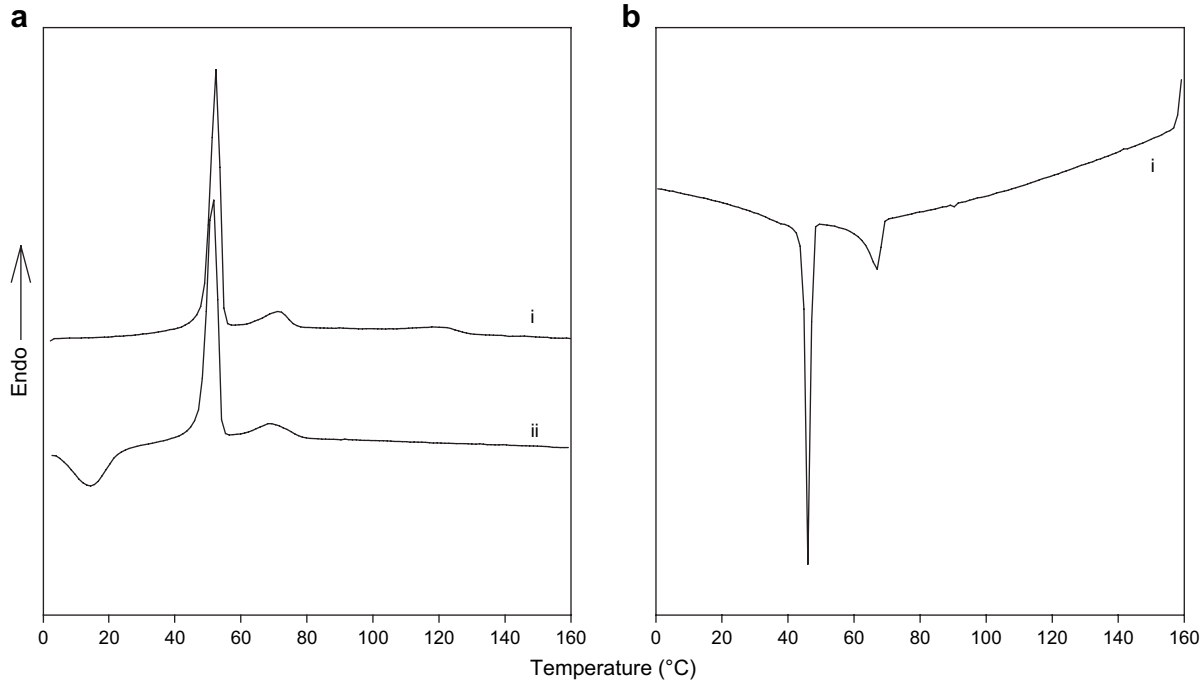

Fig. 10. DSC traces of azo-10N/PA–H at 10 °C/min, (a) heating scans and (b) cooling scan [with (i) first heating and cooling scans and (ii) second heating scan].

mesogen. The two other mixtures have similar stability, which is about 30–60 °C higher than the corresponding pure mesogen. It was also observed that, contrary to the mesogens, the azo-12N/PSS–H mixture is a little more stable than azo-10N/PSS–H.

The DSC traces for the azo-10N/PA–H stoichiometric mixture are presented in Fig. 10. The transition temperatures and their corresponding enthalpies or heat capacity increments are given in Table 3.

When the azo-10N is mixed with PA–H, the transitions observed in the pure mesogen appear at the same temperatures in the mixtures. However, the associated enthalpies are smaller for the mixtures than for the corresponding pure mesogen. These transitions and their temperatures are reproducible in subsequent scans. This can be explained by the presence of uncomplexed mesogen in these mixtures (in excess of the 50% that may be complexed), as supported by the infrared analysis and as concluded by Tork and colleagues [9,10] for LC-1,*n*N/PA–H complexes. In other words, the first two transitions may be associated with a pure mesogen phase in the phase-separated mixture. This phase is unperturbed by the presence of the polymer complex, as also observed by Tork and colleagues [9,10].

At higher temperatures, another weak transition is evident for the azo-10N/PA–H mixture that is not present in the pure mesogen. This new transition near 120 °C is weak, broad and visible only in the first heating scan, but not present in subsequent thermograms. This transition was also observed by Tork and Bazuin [8–10] for the LC-1,*n*N/PA–H mixtures (but reproducible on subsequent scans), and was concluded to be a transition between a liquid crystalline mesophase and the isotropic phase of the proton transfer complex. It is known that PA–H is subject to anhydride formation above about 140 °C [21]. Possibly, the loss of the new transition in the second scan can thus be related to the fact that the samples were previously scanned to 150 or 160 °C. Further investigations, where the scans are limited to a maximum of about 130 °C are required to clarify this. It should be mentioned that no glass transition (T_g) is visible in the thermograms of the azo-10N/PA–H mixture.

POM observations show that the phase between the first two transitions (related to the uncomplexed mesogen phase) is birefringent and fluid. Above the first transition temperature, the birefringence is interspersed with black regions, which can be associated with a homeotropic texture or with an isotropic phase. At temperatures above the second transition the

Table 3
DSC data for the stoichiometric mixtures azo-10N/P–H and azo-12N/PSS–H (obtained from second heating and first cooling thermograms at 10 °C/min)

Complex		T_1 (°C)	ΔH_1 (J/g)	T_2 (°C)	ΔH_2 (J/g)	T_3 (°C)	ΔH_3 (J/g)	T_g (°C)	ΔC_p (J g^{-1} °C^{-1})
Azo-10N/PA–H	Heat	52	18–22	68–71	2.7	125	0.8	–	–
	Cool	46	−7	64–67	−2.7	–	–	–	–
Azo-10N/PSS–H	Heat	–	–	–	–	121	1.3	38	0.28
	Cool	–	–	–	–	116	−1.2	–	–
Azo-12N/PSS–H	Heat	–	–	–	–	130	1.4	42	0.15
	Cool	–	–	–	–	120	−1.1	–	–

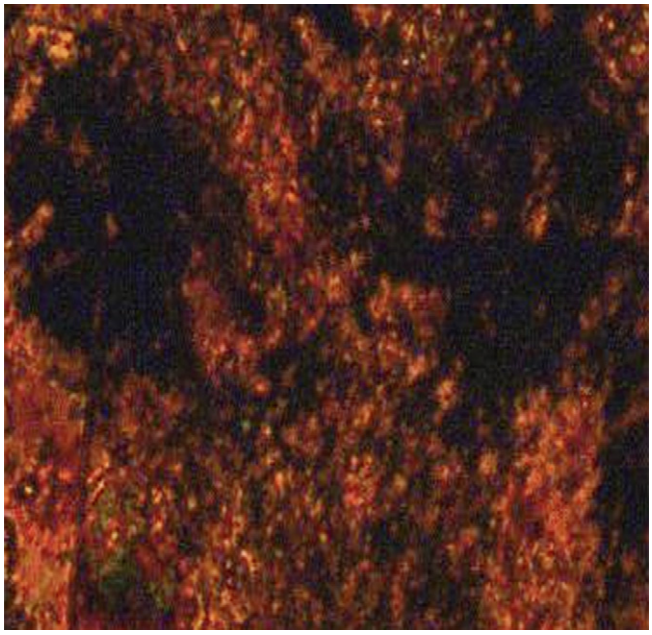

Fig. 11. Polarizing optical micrograph observed for azo-10N/PA–H mixture at 50 °C after slow cooling (3 °C/min) from the isotropic phase.

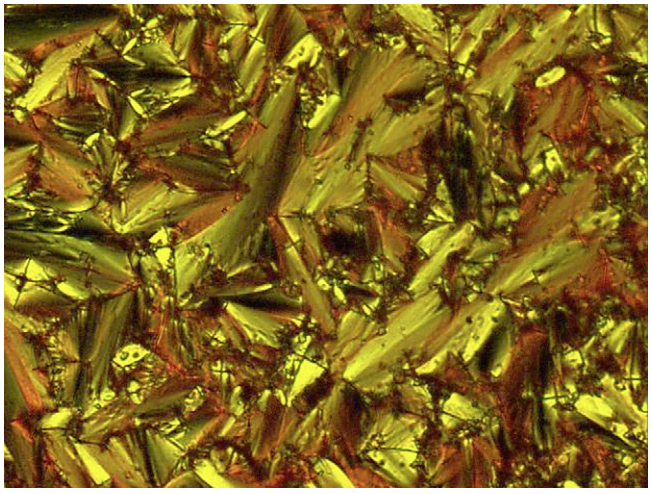

Fig. 13. Photomicrograph of a focal conic texture of azo-10N/PSS–H at 100° C after cooling (3 °C/min) from the isotropic state.

birefringence disappears, thus indicating an isotropic phase (thus, this may be responsible for the black regions between the first two transitions). This appears to contradict the presence of a liquid crystalline phase for the complex (as suggested by the first DSC heating thermogram and as observed by Tork and colleagues [9,10] for the LC-1,*n*N/PA–H mixtures). On cooling from the isotropic phase (3 °C/min), the birefringence reappears slowly in the range of 65 °C, corresponding to T_2 observed in the DSC cooling thermograms. The texture observed, even on cooling from the isotropic phase, is not well-defined, as shown in Fig. 11.

When azo-10N and azo-12N are mixed with PSS–H, the thermotropic behavior observed is very different from that of the pure mesogens. This is shown by the DSC scans in Fig. 12, with the corresponding data given in Table 3. Clearly, both complexes possess a single, low-enthalpy first-order transition at high temperatures and a glass transition near ambient temperature. The first-order peak occurs at much higher temperatures than the melting points of the pure mesogens. The temperature is higher for the stoichiometric mixture with azo-12N than with azo-10N. This transition is also visible on cooling curves, with low supercooling. The enthapy of this transition is always low. The glass transition temperatures are similar at about 40 °C for the two stoichiometric mixtures, and the corresponding ΔC_p are similar for these mixtures at about 0.2 J g^{-1} K^{-1}. To confirm the liquid crystalline nature of these complexes and to identify the phases, POM observations were made. Both mixtures are birefringent below and isotropic above this transition, which therefore corresponds to the clearing temperature of the complexes. The birefringence in these samples is reversible. In order to obtain a clear characteristic optical texture for phase identification, the mixtures are cooled slowly from approximately 10 °C above its isotropisation temperature at 3 °C/min, prior to analysis. Fig. 13 shows photomicrograph of azo-10N/PSS–H mixture under crossed polarizers. The focal conic texture developed slowly on

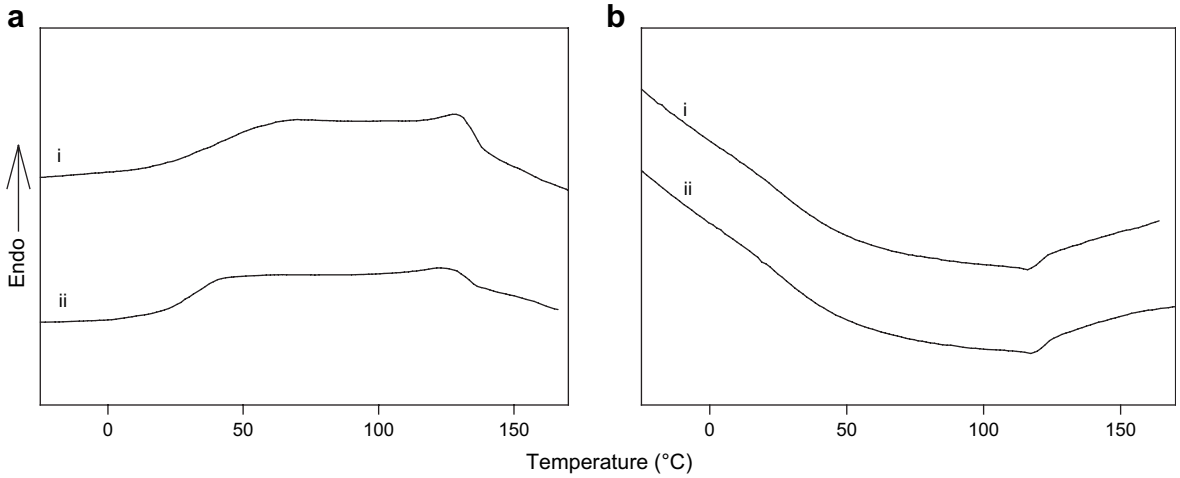

Fig. 12. DSC traces of azo-*n*N/PSS–H at 10 °C/min; (a) second heating scans and (b) first cooling scans [with (i) azo-12N/PSS–H and (ii) azo-10N/PSS–H].

cooling from the isotropic phase indicates that the mixture forms a smectic A phase in the temperature region between T_g and T_3. This texture remains essentially unaltered on cooling below T_g. This behavior could be of great interest for non-linear optics or data storage application.

3.3.3. Structural characterization

X-ray diffraction patterns for the azo-10N/PA–H mixtures at various temperatures are shown in Fig. 14a and associated data are given in Table 4. At ambient temperature, the profile is very similar to that of pure azo-10N, with several diffraction peaks at wide angles indicative of a crystalline phase and three equidistant peaks at small angles with the same intensity profile and identical lamellar spacing. At temperatures between the first and second DSC transitions, the profile is characterized by a broad peak centered at about $2\theta = 20^\circ$ and three diffraction peaks at small angles with the reciprocal spacings in the ratio 1:2:3, indicative of a smectic A or C mesophase with a layer spacing identical to that observed for the pure mesogen. These data confirm the presence of uncomplexed mesogen that is phase-separated from the polymer or complex as was observed by Tork and colleagues [9,10]. In contrast, no evidence of mesophase order is observed between the second and third DSC transitions (first scan, to which the X-ray sequence corresponds) in the azo-10N/PA–H mixture. This is in accordance with the POM observations indicating an essentially isotropic phase.

The X-ray diffractograms of the azo-10N/PSS–H mixture at various temperatures are shown in Fig. 14b and associated data are given in Table 4. At ambient temperature, the profile shows a broad halo at wide angles and two sharp and equidistant small angle diffraction peaks. Upon raising the temperature, the profiles undergo essentially no change until the isotropic phase is reached, and are reversible on cooling. These data indicate that the complex is organized as a disordered lamellar phase. In Table 4, the lamellar thicknesses calculated from the small angle diffraction peaks at ambient temperature, using the Bragg equation, are compared with the maximum molecular length calculated for the complexes.

The energy minimisation was calculated for one unit where the chromophore is perpendicular to the polymer repeat unit, with the nitrogen of amine moiety placed in the vicinity of the sulfate groups. The center-to-center distance between N of the tertiary amine moiety and the C of the carboxyl (or the S of the sulfonate) moiety is consistently found to be 4.8 ± 0.1 Å. Clearly, the measured lamellar thicknesses of the disordered birefringent phase are between one and two

Table 4
X-ray scattering data of the azo-10N/P–H mixtures at various temperatures

Temperature (°C)	Azo-10N/PA–H ($l_C = 34.2$ Å)				Azo-10N/PSS–H ($l_C = 38.5$ Å)		
	d_1 (Å)	d_2 (Å)	d_3 (Å)	d_w (Å)	d_1 (Å)	d_2 (Å)	d_w (Å)
30[a]	58.9	29.4	19.6	–	47.5	23.7	4.5
55[a]	46.5	22.9	15.3	4.5	[c]	[c]	[c]
75[a]	43.1	21.9	14.4	4.5	[c]	[c]	[c]
80[a]	[c]	[c]	[c]	[c]	46.9	23.5	4.5
100[a]	[c]	[c]	[c]	[c]	46.5	23.4	4.5
110[a]	–	–	–	4.5	[c]	[c]	[c]
130[a]	[c]	[c]	[c]	[c]	–	–	4.5
90[b]	[c]	[c]	[c]	[c]	48.5	24.3	4.5
60[b]	43.3	22.1	14.4	4.5	[c]	[c]	[c]
30[b]	55.2	31.5	24.5	–	49.1	24.5	4.5

[a] Heating.
[b] Cooling.
[c] Not measured.

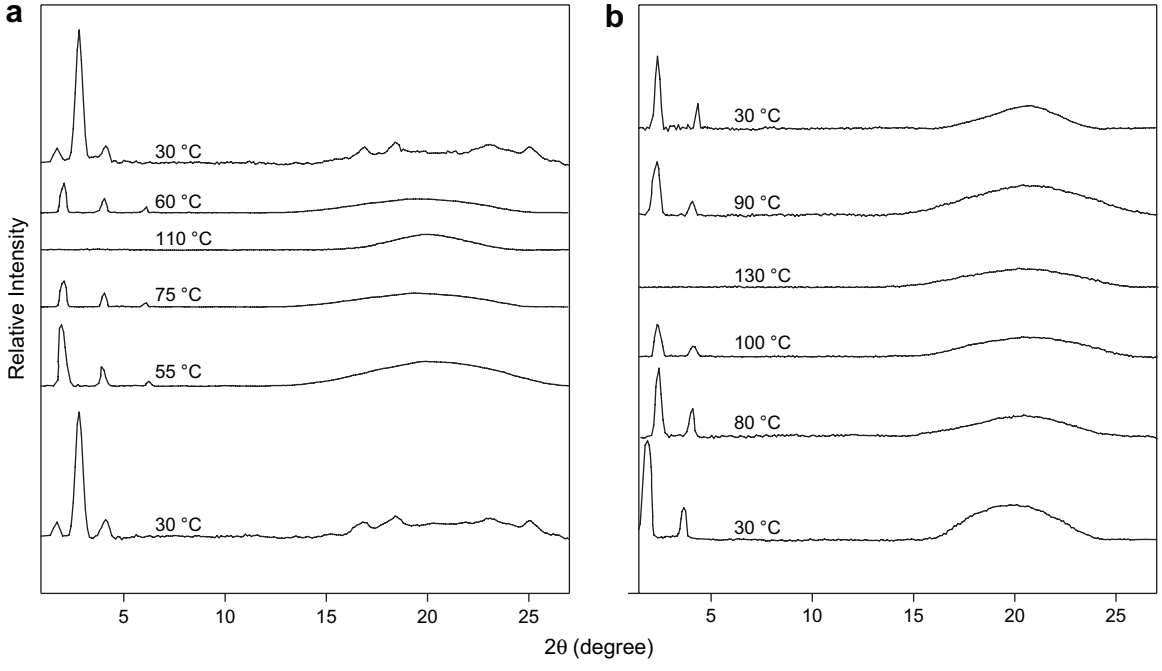

Fig. 14. X-ray diffraction profiles of (a) azo-10N/PA–H and (b) azo-10N/PSS–H obtained upon heating and cooling (in order from bottom to top).

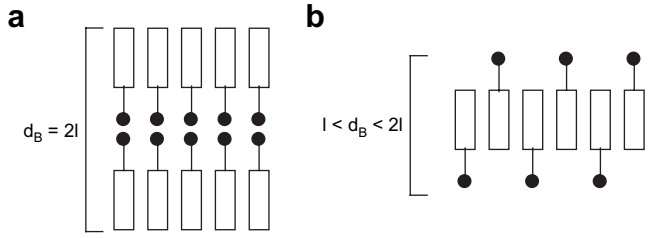

Fig. 15. Schematic representation of the arrangement of mesogen molecules in (a) bilayer (at lower temperatures) and (b) partial bilayer (at higher temperatures).

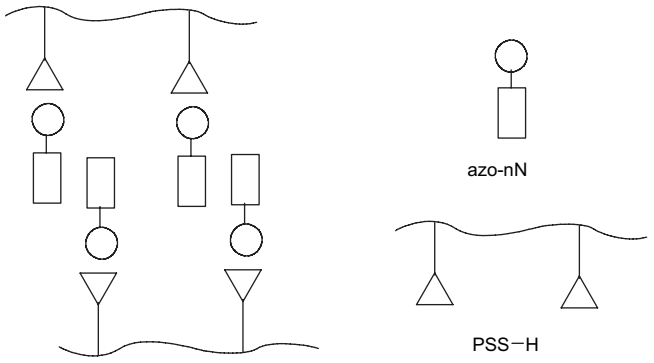

Fig. 16. Schematic representation of the arrangement of azo-*n*N/PSS–H molecules ($n = 10$, 12) in partial bilayer.

molecular lengths. This indicates that the complexes in the disordered lamellar mesophase are structurally organized into a partial or interdigitated bilayer (smectic A) or a tilted bilayer (smectic C).

4. Conclusions

In this work, two novel amine-functionalized azobenzene mesogens were prepared and studied. The thermal and structural characterization of the functionalized mesogens and their complexes were carried out by DSC, POM, X-ray diffraction, and FTIR spectroscopy.

As shown by DSC and POM, both the azo-10N and azo-12N mesogens show highly ordered structures at ambient temperature, and a disordered mesophase at higher temperatures. There is nonsignificant dependence of the transition temperature on alkyl spacer length. The X-ray diffraction data compared with the lengths of the mesogens in their most extended conformation suggest a partial bilayer S_A mesophase at higher temperatures, and a highly ordered phase, in which the molecules are stacked orthogonally in bilayers, at lower temperatures. The possible molecular arrangements for these phases are shown in Fig. 15. Similar results were reported in the literature by Brecl and Malavasic [22] for the same type of azo mesogens (with 10 and 12 C in the spacer) but diethoxy-amine functionalized (C*n*-diol). They reported that the C*n*-diol exhibits two transitions: the first one (at lower temperature) is associated with a crystal to liquid crystalline transition and the second one (at higher temperature) is due to a liquid crystalline-to-isotropic transition. The higher temperature mesophase was identified as a hexatic smectic B phase.

On mixing the neat amine-functionalized mesogens with PA–H and PSS–H at equimolar ratio, acid–base interactions take place, with proton transfer from acid to amine moieties, as confirmed by FTIR analysis. In the case of the mixture with PA–H the complexation is partial, while in the mixture with PSS–H complete proton transfer occurs.

As shown by DSC and POM, when the azo-*n*N is blended with PA–H the thermotropic behavior is not significantly affected. In contrast, by mixing the same mesogen with PSS–H the thermotropic behavior is significantly influenced and looks like the behavior observed for the azo-*n*Q/polyelectrolyte systems [11].

The equimolar azo-10N/PA–H mixture forms a biphasic system composed of a mesogen-pure phase and a phase composed of the mesogen–polymer complex. The thermal and structural characteristics of the mesogen-pure phase in the equimolar mixture are identical to those of the mesogen alone; i.e. they are not affected by the presence of the complex phase. The complex phase shows a higher temperature transition that could be the clearing point of a liquid crystalline phase of the complex (as observed by Tork and colleagues for similar mixtures with PA–H) [8,9,18,23,24]. No evidence of liquid crystalline phase of the complex was observed by POM and X-ray diffraction, although the DSC thermogram suggested a clearing transition on the first heating only. This apparent inconsistency requires further investigation.

The equimolar azo-10N/PSS–H complex is organized as a partial or interdigitated smectic A or tilted smectic C lamellar phase, similar to those observed in the azo-*n*Q/polyelectrolyte complexes [11]. The smectic–isotropic transition temperatures are higher than the mesogen corresponding transition temperatures. The models shown in Fig. 16 can be proposed for the molecular arrangement in the azo-*n*N/PSS–H system.

The study described above clearly illustrates that by mixing amorphous, commercially available polyelectrolytes with appropriate functionalized low molar mass mesogens, a disordered liquid crystalline mesophase over a very wide temperature range, can be generated, through intermolecular hydrogen bonds. It was observed that this phenomenon is considerably more evident for the complexes involving sulfonate than for carboxylate functionalities.

The importance of this work is the development of a very useful class of materials from both fundamental and practical points of view. The lability of the non-covalent interactions may offer special advantages in the development of new polymer–mesogens systems with desired properties. The relative simplicity of the synthesis of low molecular weight mesogen, the wide variety of available polyelectrolytes, the easier control of the varying molar ratios of components and the nature and strength of the intermolecular interactions provide opportunities for tailoring and control of the supramolecular SCLCPs properties. It will be of particular interest to orient the dipoles in these materials and test the stability of this orientation. The intrinsic orientation in the liquid crystalline mesophase and the high viscosity of these supramolecular SCLCPs make these compounds promising as materials for non-linear optical applications.

Acknowledgements

C.M.T. thanks Professor C. Geraldine Bazuin for providing research facilities and for helpful discussions. The financial support of NSERC (Canada) and FCAR (Québec) is gratefully acknowledged.

References

[1] Shibaev VP, Kostromin SG, Ivanov SA. In: Shibaev VP, editor. Polymers as electroattractive and photooptical media. Berlin: Springer; 1996. p. 37–110.
[2] Feringa BL, van Delden RA, Koumura N, Geertsema EG. Chem Rev 2000;100(5):1789–816.
[3] Shibaev VP, Bobrovski A, Boiko N. Prog Polym Sci 2003;28(5): 729–836.
[4] Kato T, Uryu T, Kaneuchi F, Jin C, Fréchet JMJ. Liq Cryst 2006;33 (11–12):1434–7.
[5] Kamikawa Y, Nishii M, Kato T. Mol Cryst Liq Cryst 2005;435(1): 95–105.
[6] van Ekenstein GA, Polushkin E, Nijland H, Ikkala O, ten Brinke G. Macromolecules 2003;36(10):3684–8.
[7] Uchida E, Kawatsuki N. Macromolecules 2006;39(26):9357–64.
[8] Bazuin CG, Tork A. Macromolecules 1995;28(26):8877–80.
[9] Tork A, Bazuin CG. Macromolecules 2001;34(22):7699–706.
[10] Bazuin CG, Boivin J, Tork A, Tremblay H, Bravo-Grimaldo E. Macromolecules 2002;35(18):6893–9.
[11] Tibirna CM, Bazuin CG. J Polym Sci Part B Polym Phys 2005;43(23): 3421–31.
[12] Danis PO, Karr DE. Macromolecules 1995;28(25):8548–51.
[13] Vogel A. Vogel's textbook of practical organic chemistry. 4th ed. New York: Longman; 1978.
[14] Ujiie S, Iimura K. Polym J 1993;25(4):347–54.
[15] Zundel G. Hydration and intermolecular interaction. New York: Academic Press; 1969.
[16] Fan XD, Bazuin CG. Macromolecules 1995;28(24):8209–15.
[17] Bazuin CG, Fan XD, Lepilleur C, Prud'homme RE. Macromolecules 1995;28(4):897–903.
[18] Tork A. Ph.D. thesis. Québec: Laval University; 1998.
[19] Navarro-Rodriguez D, Guillon D, Skoulios A, Frère Y, Gramain Ph. Macromol Chem 1992;193(12):3117–28.
[20] Pasto DJ, Johnson CR. Organic structure determination. Englewood Cliffs, NJ: Prentice Hall; 1969.
[21] Dong J, Ozaki Y, Nakashima K. Macromolecules 1997;30(4): 1111–7.
[22] Brecl M, Malavasic T. J Polym Sci 1997;35(14):2871–88.
[23] Bazuin CG, Brandys FA. Chem Mater 1992;4(5):970–2.
[24] Tremblay H. M.Sc. thesis. Québec, Canada: Laval University; 2000.